Please cite this article in press as: Sun et al., Single-Molecule Kinetics of the Eukaryotic Initiation Factor 4AI upon RNA Unwinding, Structure (2014), http://dx.doi.org/10.1016/j.str.2014.04.014

Structure
Article

Single-Molecule Kinetics of the Eukaryotic Initiation Factor 4AI upon RNA Unwinding

Yingjie Sun,[1] Evrim Atas,[1] Lisa M. Lindqvist,[2,3,5] Nahum Sonenberg,[3] Jerry Pelletier,[3] and Amit Meller[1,4,*]
[1]Department of Biomedical Engineering, Boston University, Boston, MA 02215, USA
[2]Department of Medical Biology, The University of Melbourne, Parkville, VIC 3010, Australia
[3]Department of Biochemistry and The Rosalind and Morris Goodman Cancer Research Center, McGill University, Montreal, QC H3G 1Y6, Canada
[4]Faculty of Biomedical Engineering, The Technion, Haifa 32000, Israel
[5]Present address: Division of Cell Signaling and Cell Death, The Walter and Eliza Hall Institute of Medical Research, Parkville, VIC 3052, Australia
*Correspondence: ameller@bu.edu
http://dx.doi.org/10.1016/j.str.2014.04.014

SUMMARY

The eukaryotic translation initiation factor 4AI (eIF4AI) is the prototypical DEAD-box RNA helicase. It has a "dumbbell" structure consisting of two domains connected by a flexible linker. Previous studies demonstrated that eIF4AI, in conjunction with eIF4H, bind to loop structures and repetitively unwind RNA hairpins. Here, we probe the conformational dynamics of eIF4AI in real time using single-molecule FRET. We demonstrate that eIF4AI/eIF4H complex can repetitively unwind RNA hairpins by transitioning between an eIF4AI "open" and a "closed" conformation using the energy derived from ATP hydrolysis. Our experiments directly track the conformational changes in the catalytic cycle of eIF4AI and eIF4H, and this correlates precisely with the kinetics of RNA unwinding. Furthermore, we show that the small-molecule eIF4A inhibitor hippuristanol locks eIF4AI in the closed conformation, thus efficiently inhibiting RNA unwinding. These results indicate that the large conformational changes undertaken by eIF4A during the helicase catalytic cycle are rate limiting.

INTRODUCTION

The biological function of most enzymes is closely related to their dynamic structural properties and to their ability to switch between different conformations upon substrate binding and modification. Characterization of their dynamic properties can thus provide vital information to understanding how these enzymes function and what may lead to malfunctioning events. Moreover, this information can inspire the design of novel molecular inhibitors or stimulators intended to regulate their activity with potentially therapeutics properties. A case in point is the eukaryotic initiation factor 4AI (eIF4AI), an RNA helicase and a core member of the eIF4F complex, which mediates 5′ m^7GpppN cap binding and mRNA unwinding (Sonenberg and Hinnebusch, 2009). This enzyme catalyzes ATP-driven unwinding of secondary structure at the 5′ UTR of the mRNA required for translation initiation and ribosome recruitment on most capped mRNA transcripts (Sonenberg and Hinnebusch, 2009). An alternative form of translation initiation occurs independent of the 5′ end by recruitment of 40S ribosomal subunits to internal ribosome entry sites (IRESs)—a process that in many cases also involves RNA unwinding by eIF4AI (Pestova et al., 2001).

eIF4AI is the prototypical member of the DEA(D/H)-box RNA helicase family and is one of the more abundant translation initiation factors, present at ~3 copies/ribosome (Duncan and Hershey, 1983; Galicia-Vázquez et al., 2012). DEAD-box proteins share highly conserved amino acid sequence motifs and a helicase core of two flexibly linked domains. In addition to interacting with double-stranded RNA and single-stranded RNA (ssRNA) at the canonical RNA binding site within the core, eIF4AI also interacts with other initiation factors, such as the scaffolding protein eIF4G (Andreou and Klostermeier, 2014; Feoktistova et al., 2013; Oberer et al., 2005) and the RNA-binding factors, eIF4H and eIF4B (Rogers et al., 2001b). Crystallographic analyses have revealed that related DEAD-box proteins, such as Vasa (Sengoku et al., 2006), eIF4AIII (Bono et al., 2006), Mss116p (Del Campo and Lambowitz, 2009), DbpA (Henn et al., 2010), CYT-19 (Grohman et al., 2007), and YxiN (Theissen et al., 2008), adopt a compact conformation in the presence of RNA and the ATP analog AMPPNP. ATP binding and phosphate release are thought to control opening and closing of the helicase core (Andreou and Klostermeier, 2012). This movement coordinates RNA binding and ATPase activity and is thus central to the function of DEAD-box helicases. However, the relationship between the helicases conformational transition timescales and their unwinding activity remains vague, because this question necessitates direct observation of the helicases' conformation over time. In particular, X-ray crystallography indicated that ssRNAs may become "kinked" when eIF4AI adopts a close conformation, suggesting that this might be related to the enzymes' unwinding capabilities (Bono et al., 2006; Del Campo and Lambowitz, 2009; Sengoku et al., 2006). However, ssRNA kinks can only explain local RNA melting (~3 nt), whereas DEAD box

Please cite this article in press as: Sun et al., Single-Molecule Kinetics of the Eukaryotic Initiation Factor 4AI upon RNA Unwinding, Structure (2014), http://dx.doi.org/10.1016/j.str.2014.04.014

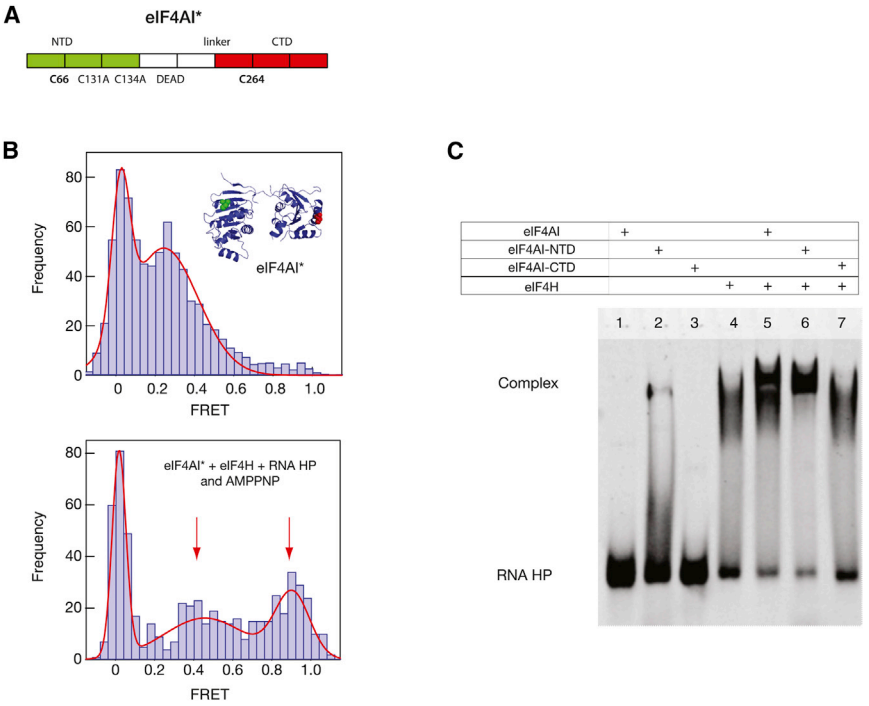

Figure 1. Binding of RNA and AMPPNP Induces a Conformational Change in eIF4AI

(A) A schematic diagram of eIF4AI* mutants consisting of two cysteine-to-alanine substitutions (C131A, C134A) and two native cysteines (C66, C264) used for coupling a donor-acceptor FRET dye pair (Cy3-Cy5).

(B) FRET histograms for the labeled eIF4AI* constructs. Top panel shows the FRET histogram for eIF4AI* (N- and C-terminal domains are labeled) in the absence of any ligands. Bottom panel shows FRET histogram of eIF4AI* upon addition of RNA HP and AMPPNP.

(C) EMSA of full-length eIF4AI and NTD- and CTD-truncated mutants binding RNA in the presence or absence of eIF4H.

helicases, such as eIF4AI, can unwind longer RNA duplexes (Rogers et al., 2001a).

We have recently shown that the eIF4AI/eIF4H complex can bind directly to RNA loop structures and repetitively unwind short RNA hairpins (Sun et al., 2012). These results indicated that assembly of eIF4AI/eIF4H on the RNA hairpin substrate, and subsequent unwinding of its duplex regions, can be significantly enhanced by stable binding of the proteins to single-stranded loop domains longer than a critical minimum length of 6 nt. Here, we focus our attention on eIF4AI's conformational transitions during RNA unwinding. By labeling the helicase with a donor-acceptor fluorophore pair, we directly probe its conformational transitions during ATP binding and hydrolysis using single-molecule fluorescence resonance energy transfer (sm-FRET) methods. We find that in the presence of eIF4H, eIF4AI repetitively unwinds the RNA hairpin substrate by transitioning between an "open" and a "closed" conformation using the energy derived from ATP hydrolysis. The transitions between these two conformations involve interdomain distance changes of nearly 2 nm and on average take 1.7 s for a complete cycle (closed-open-closed). We further show that the natural product hippuristanol (Bordeleau et al., 2006) inhibits the helicase activity of eIF4AI by locking it into the closed conformation.

RESULTS

eIF4AI/eIF4H/RNA Hairpin Complex Formation Involves a Transition from an "Open" to a "Closed" Conformation

Site-directed mutagenesis was used to generate a cysteine-less eIF4AI mutant (C66A, C131A, C134A, C264A). In addition, eIF4A variants that harbored only two cysteine residues in either the NTD at position 66 and 131 (C134A, C264A), two cysteines in the CTD at position 264 and 403 (C66A, C131A, C134A, A403C), or a single cysteine in each of the two domains at position 66 and 264 (C131A, C134A), shown schematically in Figure 1A (detailed schematic diagrams of all mutants are shown in Figure S7 [available online]). We refer to these three full-length eIF4AI mutants as eIF4AI*^{N}, eIF4AI*^{C}, and eIF4AI*, respectively. These mutants showed comparable helicase activity in vitro with the wild-type eIF4AI (Figures S6 and S7). The cysteine residues were labeled with donor and acceptor dyes (Cy3 and Cy5 maleimide derivatives, respectively) with >95% labeling efficiency for single-molecule analyses.

Sm-FRET burst analyses of the purified-labeled proteins were used to determine the FRET level distributions, which showed two clear peaks both for eIF4AI* and for eIF4AI*^{N} and eIF4AI*^{C}. In all cases we observe a peak around $F = 0$, which simply represents proteins labeled with either a single or two donor molecules instead of a donor-acceptor pair, and a second "nonzero" peak. This second peak varied widely among the three eIF4AI mutants: the eIF4AI* mutant exhibited a peak at low FRET levels $F = 0.30 \pm 0.04$ (Figure 1B, top panel). The two other mutants displayed peaks at $F = 0.80 \pm 0.02$ or $F = 0.90 \pm 0.02$ (eIF4AI*^{N} or eIF4AI*^{C}, respectively, as shown in Figure S1). The nonzero FRET peak can be used to estimate the donor-acceptor distance. Specifically, the high FRET values obtained for the controls eIF4AI*^{N} and eIF4AI*^{C} agree very well with the expected distance between the two dyes (4.8 and 4.2 nm, respectively) using their known Förster radius of $R_0 = 6$ nm (Roy et al., 2008).

The relatively low FRET state of the doubly labeled mutant eIF4AI* is consistent with the "open" state conformation of yeast and human eIF4A homologs (Caruthers et al., 2000; Chang et al., 2009). Incubation of eIF4AI*, eIF4H, and the RNA hairpin (HP) with 2 mM nonhydrolysable ATP analog, AMPPNP, induced the formation of an additional FRET state having a much higher value (Figure 1B, bottom; $F = 0.80 \pm 0.04$). This result indicates that binding of AMPPNP induces closure of eIF4AI to a more compact conformation in which the NTD and CTD of the protein are brought closer to each other. We define this state as the "closed" eIF4AI conformation. As can be seen from Figure 1B, despite the fact that AMPPNP is added at saturating concentration levels, only ~50% of the bursts consisting of a

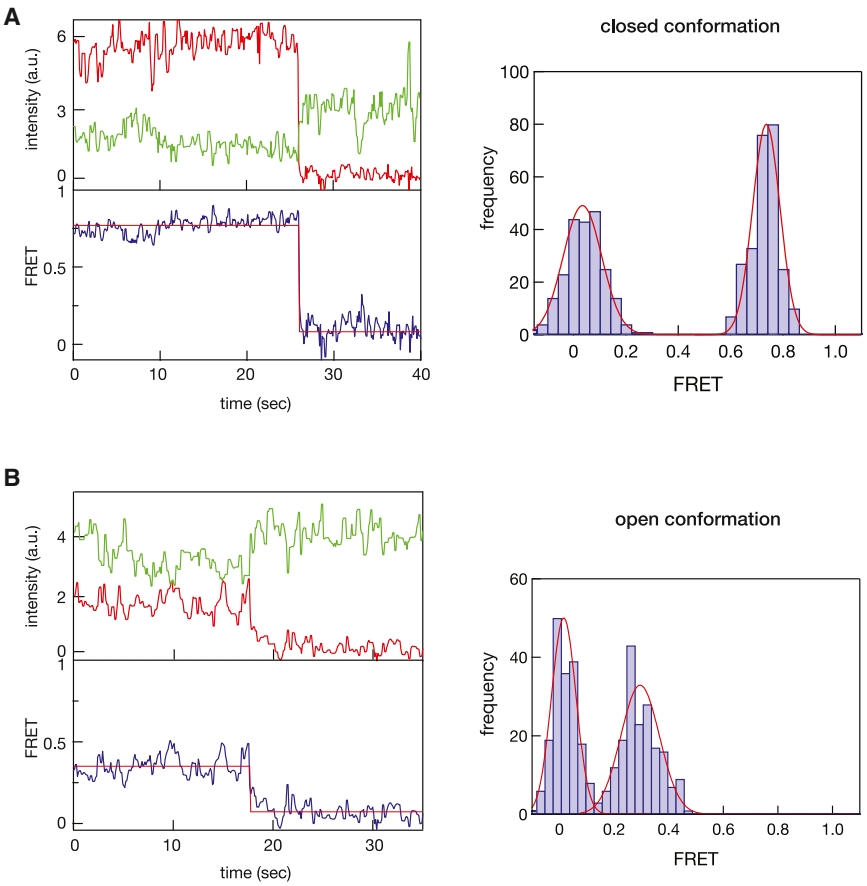

Figure 2. Direct and Real-Time Observation of the Open and Closed Conformations of eIF4AI*

(A and B) The labeled eIF4AI and the accompanying reagents (RNA HP, eIF4H, and AMPPNP) were encapsulated in 200 nm vesicles and FRET measurements performed. (A) A typical single-molecule FRET trace exhibiting "closed" conformation (left panel), yielding high FRET state (histogram on right panel). (B) A typical single-molecule trace exhibiting "open" conformation (left panel), yielding low FRET state (right panel histogram). The FRET histograms (right panels) include >100 single-molecule traces in each case.

donor-acceptor pair showed high FRET value. We note that the burst analysis cannot distinguish between free eIF4AI or eIF4AI present in an eIF4AI/eIF4H/RNA hairpin complex. We postulate that the contribution to the lower FRET peak comes from uncomplexed (free) eIF4AI molecules remaining at thermal equilibrium with the complexed form.

We further used an electrophoretic mobility shift assay (EMSA) to resolve the complex formed in the presence of eIF4H and an RNA HP molecule. To this end, we generated N-terminal (eIF4A-NTD, residues 1–244) and C-terminal (eIF4A-CTD, residues 237–406) domain truncation mutants. Incubation of wild-type eIF4AI or the truncation mutants with the RNA HP substrate showed weak complexes or none at all (Figure 1C, lanes 1–3). In contrast, in the presence of eIF4H, both full-length eIF4AI and eIF4A-NTD formed a complex with RNA HP, indicated by the high FRET state in Figure 1B (see arrow), whereas this was not observed with eIF4A-CTD (Figure 1C, compare lane 7 to lanes 4–6). These results suggest that eIF4H binds to the N-terminal domain of eIF4AI when RNA HP is present.

Because the burst analysis provides only diffusion limited "snapshots" of the conformational state of eIF4AI, it does not inform on the conformational transitions timescales. Specifically, we wanted to characterize the stability of the eIF4AI/eIF4H/RNA HP complex upon AMPPNP binding. To this end, we encapsulated labeled eIF4AI and the accompanying substrates and cofactors (RNA HP, eIF4H, and AMPPNP) into lipid vesicles (DMPC) at the same stoichiometric ratios used for single-molecule analysis of individual complexes (see the Experimental Procedures). On average, the relatively small vesicle size in conjunction with the low reagent concentration used during vesicle extraction ensures the inclusion of a single eIF4AI molecule per vesicle. A small fraction of the lipid molecules contained a biotin moiety to facilitate surface immobilization for total internal reflection fluorescence (TIRF) imaging—obviating the need to induce further modifications to the RNA substrate or protein. Acquiring the donor and acceptor intensity traces versus time for a set of >500 individual complexes indicated that the complexes exist in only one of two states: the "open" (low FRET) or the "closed" (high FRET) state, rather than dynamically fluctuating between the two (Figure 2). By way of example, we present a trace illustrating a situation in which eIF4AI* exhibits a high FRET level ("closed" conformation) for a period of >25 s, after which time the acceptor dye photobleaches (Figure 2A), and a trace showing eIF4AI* exhibits low FRET ("open" conformation) for a period of >17 s (Figure 2B). Importantly, in none of our single molecule traces did we observe transitions between the two states in the presence of AMPPNP.

eIF4AI Undergoes Open-to-Closed Conformational Transitions during RNA Unzipping

Substituting AMPPNP with ATP in the FRET assays resulted in rapid and reversible FRET transitions between two distinct levels of similar FRET values to the closed and open conformations registered in the presence or absence of AMPPNP. First, burst analysis was used to characterize thousands of complexes in the presence of ATP. These results indicate that the closed conformation F = 0.72 ± 0.02 is approximately 2-fold more populated compared to the open conformation F = 0.27 ± 0.04 (Figure 3A). The burst analysis measurements do not inform on the actual transition timescale between the two states and may in fact result from either static or dynamic equilibrium between the two states. To resolve this question, we encapsulated eIF4AI with eIF4H, ATP, and RNA HP in lipid vesicles and performed sm-FRET measurements. A typical

Please cite this article in press as: Sun et al., Single-Molecule Kinetics of the Eukaryotic Initiation Factor 4AI upon RNA Unwinding, Structure (2014), http://dx.doi.org/10.1016/j.str.2014.04.014

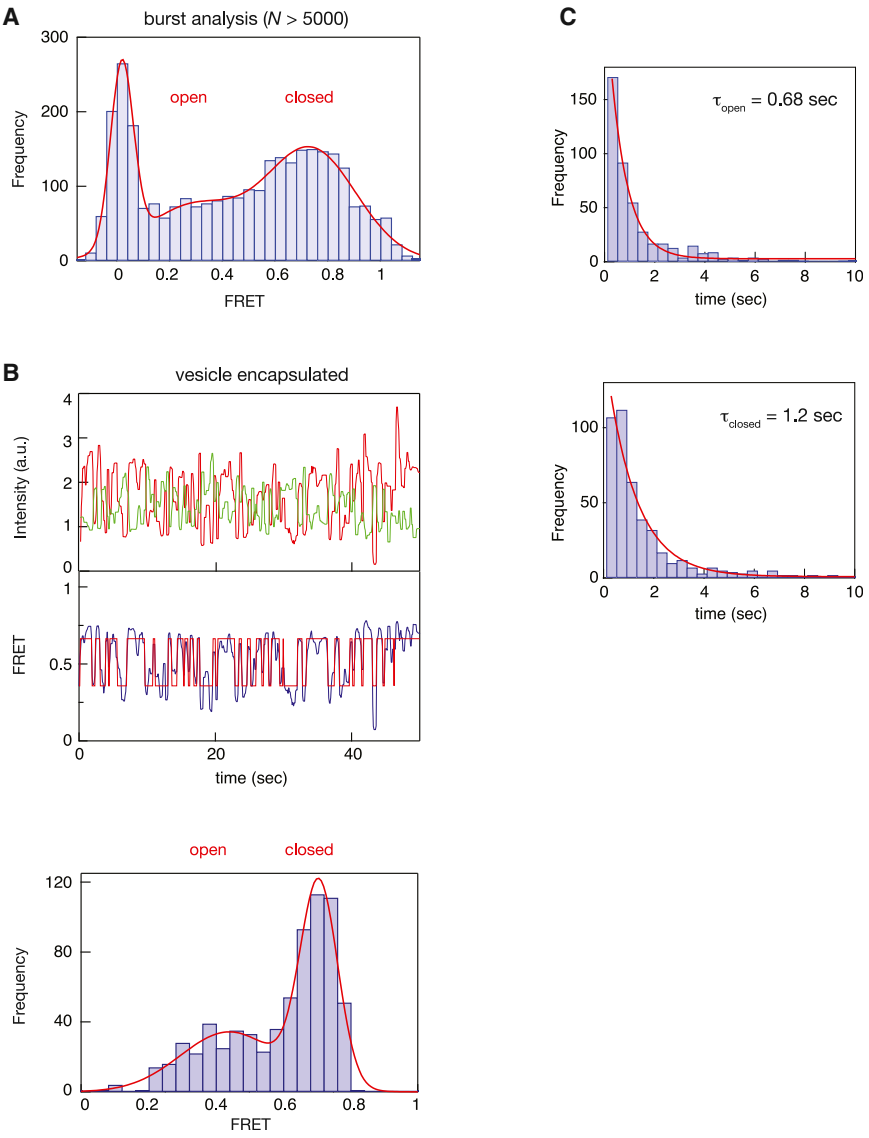

Figure 3. eIF4AI* Undergoes Open-to-Closed Conformational Transitions during RNA Unzipping

(A and B) FRET transitions between open and closed conformations are observed in the presence of ATP. (A) FRET histogram obtained using burst analysis (n > 5,000) show two nonzero FRET peaks at F = 0.72 ± 0.02 (closed conformation), and F = 0.27 ± 0.04 (open conformation). (B) Typical sm-FRET trace when eIF4AI* is encapsulated with eIF4H, RNA HP, and ATP in a vesicle (top panel). Multiple conformational transitions between open-closed states are observed (bottom panel).

(C) Statistical analysis of transitions yield dwell times for both states with characteristic timescales τ_{open} = 0.68 ± 0.05 s and τ_{closed} = 1.20 ± 0.05 s.

sm-FRET trace and the calculated FRET level as a function of time are shown in Figure 3B. We observe multiple slow conformational transitions between the two FRET levels over a span extending beyond 2 min. Each oscillation of the FRET trace between high and low levels represents a single "open" and "closed" cycle of eIF4AI. A hidden Markov model (HMM) analysis (see the Experimental Procedures) (McKinney et al., 2006) was used to extract the dwell times of the two states characterized by the "closed time" (dwell time at high FRET level) and the "open time" (dwell time at low FRET level). Statistical analysis of hundreds of these transitions revealed exponential distributions of the dwell times for each state (Figure 3C), with characteristic timescales, τ_{open} = 0.68 ± 0.05 s and τ_{closed} = 1.20 ± 0.05 s. The 2-fold increase in dwell time of eIF4AI in the closed state correlates well with the burst analysis amplitudes in Figure 3A. Notably, in the absence of eIF4H, and otherwise under identical conditions, we have not observed conformational transitions of eIF4AI during the 2 min span of our single molecule observations, indicating that the helicase exhibits weak activity without its cofactors.

The dynamic transitions between eIF4AI conformations, characterized in Figures 3B and 3C, conform to a simple, first-order, two-state kinetic cycle, involving ATP binding (open to closed) and ATP hydrolysis and phosphate release (closed to open). Notably, the two timescales τ_{closed} and τ_{open} measured for the conformational dynamics of eIF4AI are practically indistinguishable from the "waiting" and "unwinding" timescales, respectively, that were previously reported using the eIF4AI/eIF4H complex and labeled RNA HP (Sun et al., 2012). This striking observation was confirmed by repeating our measurements using a FRET-labeled RNA HP and unlabeled mutant eIF4AI* (Figure S2). This experimental setup allows us to correlate the open eIF4AI conformation with an unwound RNA hairpin state and the closed eIF4AI conformation with a closed hairpin state. A transition from a FRET value 0.4 to 0.8 corresponds to a distance change of ~2 nm by eIF4AI, which can induce destabilization (or "unzipping") of an RNA duplex of ~15 bp long (ΔG = −18 kcal/mol). In control experiments using eIF4AI*, we did not observe conformational transitions when either ATP or RNA HP was absent.

To rule out the possibility that the observed conformational changes were due to intradomain interactions, we performed single-molecule experiments with double-labeled eIF4AI^{*N} and eIF4AI^{*C}, which had both donor and acceptor in the same domain (Figure S3). The results revealed only small FRET changes in both NTD and CTD, with FRET levels remaining mostly high throughout the experiment. Taken together, our data suggest that hairpin unzipping and eIF4AI's large conformational transitions are tightly coupled and involve movements of the NTD with respect to the CTD.

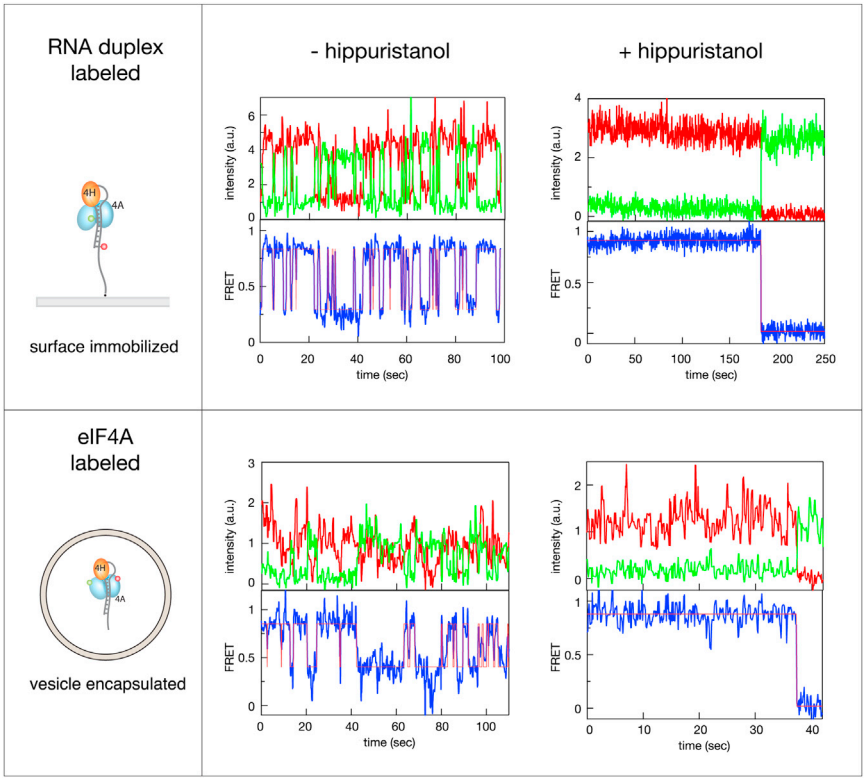

Figure 4. Hippuristanol Inhibits eIF4AI Unwinding by Trapping It in the Closed Conformation

Top panel: a typical sm-FRET trace for unwinding of double-labeled RNA hairpin with eIF4AI/eIF4H complex in the absence of hippuristanol (left). Multiple FRET states show repetitive unwinding. The addition of 10 μM hippuristanol completely inhibits these oscillations, trapping the RNA HP in its closed state (right). Bottom panel: a typical FRET trace RNA HP unzipping and labeled eIF4AI* in the absence (left) and presence of hippuristanol (right).

Hippuristanol Inhibits eIF4AI Unwinding by Locking It in the Closed Conformation

The natural product hippuristanol targets eukaryotic translation initiation factor eIF4AI. It was identified as a translation inhibitor using a high-throughput screen designed to separate compounds that specifically target cap-dependent translation (Bordeleau et al., 2006). Hippuristanol inhibits the RNA binding activity of eIF4AI in vitro and in vivo (Bordeleau et al., 2006; Lindqvist et al., 2008) without interfering with ATP binding to eIF4AI. It is therefore an ideal test molecule to validate our activity model, where the conformational dynamics of eIF4AI are coupled to RNA duplex unwinding. Bulk titration assays performed with increasing amounts of hippuristanol revealed that when the hippuristanol concentration was 5-fold higher than eIF4AI, complete inhibition of helicase activity was obtained (Figure S4A). Notably, in our assays, hippuristanol does not inhibit the binding activity of eIF4AI/eIF4H complex to RNA hairpin (Figure S4B), presumably because of the strong binding of eIF4H to the RNA loops (Sun et al., 2012), mediating binding of eIF4AI to its RNA substrate.

FRET results obtained with AMPPNP (Figure 2) suggested that binding of this ATP analog induces eIF4AI to undergo a conformational change from an open to a closed state. In addition, the results in Figure 3 suggest that ATP hydrolysis triggers the transition from the closed to the open state, as well as RNA unzipping. Based on this, and the known inhibitory characteristics of hippuristanol, we postulated that hippuristanol should not interfere with the first transition but would prevent ATP hydrolysis and thereby stall the unzipping process. To test this hypothesis, we first performed an sm-FRET study with double-labeled RNA HP as previously reported (Sun et al., 2012). Typical sm-FRET traces are shown in Figure 4. In the absence of hippuristanol, FRET oscillations are clearly visible, corresponding to the opening and closing of the RNA HP. However, upon addition of hippuristanol, these oscillations were inhibited, locking the RNA HP at the high FRET, closed state (top right panel). Sm-FRET vesicle analysis of doubly labeled eIF4AI* in the absence and presence of hippuristanol are shown in the bottom panel of Figure 4. Although these data were somewhat "noisier" than the data obtained with labeled RNA HP FRET, we clearly observed that in the presence of hippuristanol, eIF4AI is locked at the high FRET closed conformation. Further analysis revealed that less than 1% of the traces collected (n > 500) represented conformational changes in the presence of hippuristanol, whereas >11% showed oscillations without it.

DISCUSSION

In this study we combined two sm-FRET analyses methods to characterize the conformational dynamics of eIF4AI during RNA unwinding. Sm-FRET burst analysis provided "snapshots" of the characteristic FRET states of thousands of individual molecules within a relatively short period of time, thus permitting efficient and accurate determination of the representative FRET values under various conditions. In contrast, vesicle encapsulation of individual eIF4AI/eIF4H/RNA complexes allowed direct measurement of the dynamics (timescales) of any conformational changes of eIF4AI over time. But the last method is extremely time consuming. In the presence of ATP, we observe rapid transitions of eIF4AI between low and high FRET levels. These transitions were not observed when ATP was substituted with nonhydrolyzable AMPPNP molecules. These measurements, combined with single-molecule studies of FRET-labeled RNA molecules, allowed us to relate enzyme conformational timescales with RNA unwinding dynamics. Consolidating our results into a simplified coherent picture (Figure 5), we propose that ATP binding to eIF4AI induces a transition from its open conformation to the closed conformation. In the closed

Please cite this article in press as: Sun et al., Single-Molecule Kinetics of the Eukaryotic Initiation Factor 4AI upon RNA Unwinding, Structure (2014), http://dx.doi.org/10.1016/j.str.2014.04.014

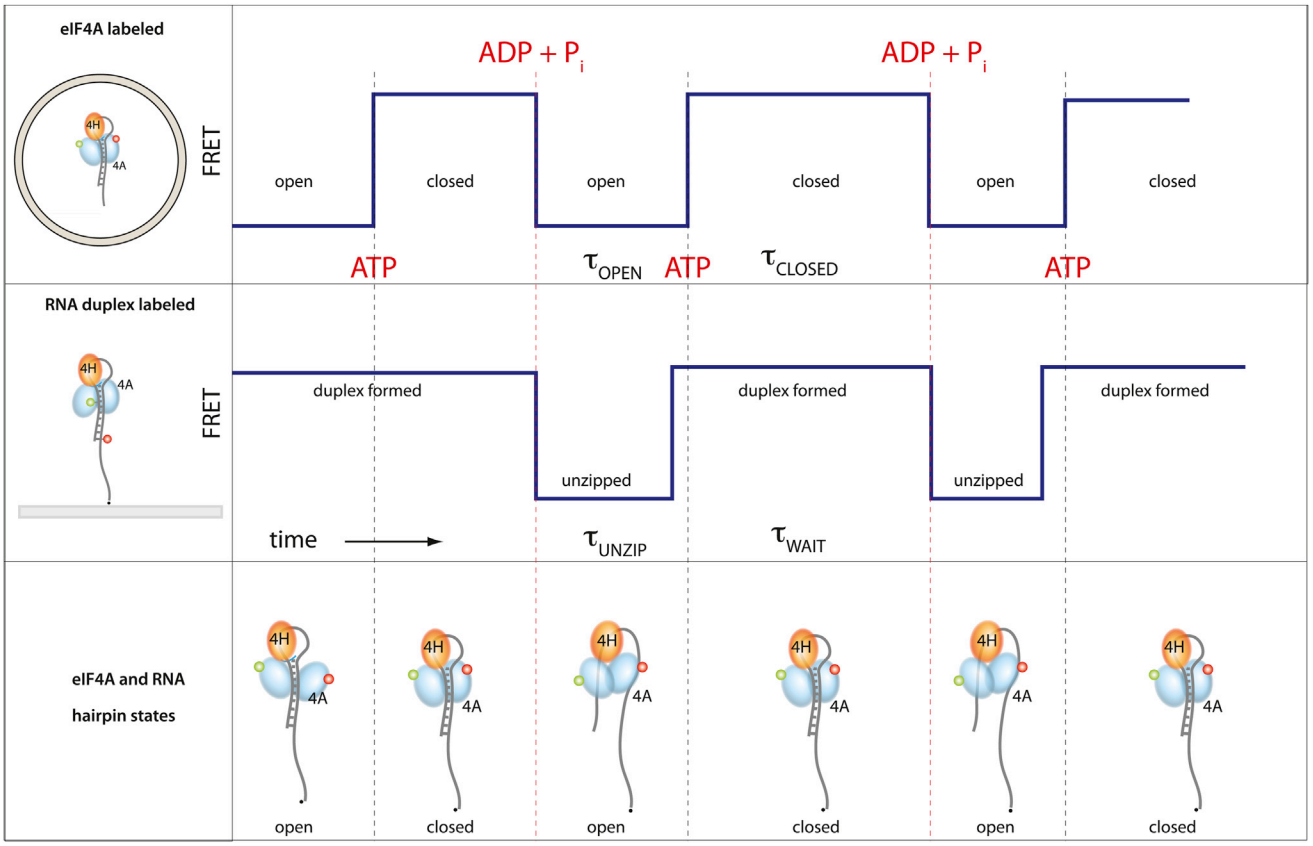

Figure 5. A Schematic Illustration of the Proposed Steps during Hairpin Binding and Stem Unzipping by the eIF4AI/eIF4H Complex

In solution, eIF4AI adopts an open conformation. eIF4AI binding to the hairpin is mediated by eIF4H loop binding. Upon ATP binding, eIF4AI adopts the closed conformation, and upon ATP hydrolysis, eIF4AI returns to the open conformation, which also induces RNA duplex unzipping. The RNA strand bound transiently to the CTD of eIF4AI is then released and the duplex quickly reanneals.

conformation state, both the NTD and CTD are free to bind to an RNA strand. ATP hydrolysis stimulates the transition to the open state of the enzyme, while simultaneously unzipping the RNA strand. Thereafter, the RNA strand is released and eIF4AI is ready to bind a new ATP molecule. In the presence of eIF4H, this process is capable of repeating itself many times, an event that results in persistent unzipping of short RNA hairpins (up to ~12 bp). The sm-FRET dwell-time distributions of eIF4AI conformational dynamics indicate that 5% of the unwinding/waiting events show total dwell time of less than 0.2 s with a median value of unwinding and waiting ~1 s. These results are consistent with recent theoretical model (Shah et al., 2013) suggesting that the average time between initiation events on a given mRNA molecule ranges from 4 (5%) to 233 s (95%), with a median value of 40 s.

eIF4H contains an RNA recognition motif (RRM) with sequence homology to another accessory protein, eIF4B (Richter-Cook et al., 1998). NMR studies showed that in the absence of RNA the C-terminal domain of eIF4AI interacts with both the middle domain of eIF4G (Oberer et al., 2005) and eIF4H (Marintchev et al., 2009). Moreover, single-molecule FRET assays were used to measure the kinetics of assembly of eIF4E-eIF4G1-eIF4A-mRNA (O'Leary et al., 2013). Our EMSA results indicate that in the presence of the RNA HP, eIF4H binds stronger to the N-terminal domain of the truncated eIF4AI, indicating that substrate binding may play a role on the eIF4AI-eIF4H-RNA complex structure. eIF4B, in conjunction with the scaffolding protein eIF4G, was previously shown to stimulate RNA unwinding by eIF4A (Rogers et al., 2001b). We demonstrate that eIF4H binds to the RNA loop and interacts with the NTD of eIF4AI in order to facilitate repeated open-to-closed conformational transitions (fueled by ATP hydrolysis). RNA unwinding of short hairpins is achieved with these repeated transitions. It would be interesting to determine if eIF4B would behave the same way or if they increase the helicase activity of eIF4AI by district mechanisms. Our model rationalizes why eIF4AI, and in general all DEAD-box helicases, do not act as highly processive helicases but rather induce local RNA unzipping (Jankowsky and Putnam, 2010; Yang et al., 2007). Even though the closed conformation is observed with the nonhydrolyzable ATP analog AMPPNP, ATP hydrolysis is required to catalyze RNA unwinding and in the presence of excess ATP, the repetitive conformational changes facilitate continuous unwinding. The correlation between the timescales of the switching from open to the closed states and repetitive unwinding kinetics indicate that large conformational changes are the rate-limiting step in the overall helicase catalytic cycle.

EXPERIMENTAL PROCEDURES

RNA Substrates

DNA and RNA oligonucleotides were purchased from IDTDNA and Dharmacon, respectively. They are chemically synthesized, modified, and high-performance liquid chromatography purified. The structure and sequence of RNA/DNA duplexes used in this study are shown in Figure S5. The RNA/DNA hairpin substrate included a 12-nt-long loop and a 12 bp stem region.

Electrophoretic Mobility Shift Assays

EMSAs were performed in binding buffer (20 mM Tris-HCl [pH 7.5], 50 mM KCl, 2.5 mM $MgCl_2$, and 1 mM DTT). Reactions containing the indicated proteins and Cy5-labeled RNA were performed at room temperature for 30 min. The single-stranded overhang region of the RNA consisted of 23 nt, and the Cy5 fluorophore was located at the 5′ end. Samples were loaded onto 7.5% nondenaturing polyacrylamide gel and following electrophoresis, gels were scanned for Cy5 emission using a Pharos FX Scanner (BioRad).

Site-Directed Mutagenesis of eIF4AI

Proteins were expressed and purified as previously described (Sun et al., 2012). Individual cysteine residues within eIF4AI were mutated to alanines by PCR-mediated mutagenesis. Generation of truncation mutants was performed in accordance with the Quikchange protocol (Agilent). eIF4AI-NTD (amino acids [aa] 1–244) was constructed by introducing a stop codon after aa 244. For eIF4A-CTD (aa 237–406), an NdeI-restriction site (CATATG) was introduced after the coding region for aa 1–234. A second NdeI site was present within the 5′ UTR of the cDNA clone, and cleavage by NdeI followed by religation lead to removal of aa 1–234. Correct sequences were confirmed for all constructs.

Double Labeling and Purification of eIF4AI Mutants

Proteins were labeled by incubating with a mixture of Cy3-maleimide (donor) and Cy5-maleimide (acceptor) overnight at 4°C. Protein concentrations were 2 mg/ml and dyes were used at concentrations of at least 5 fold molar excess with respect to the protein. The reducing agent tris(2-carboxyethyl)phosphine (TCEP) was added to the reaction at 2 mM to reduce any disulfides in the protein sample. Free dyes were removed from the labeled sample using Q Sepharose (GE Healthcare). After loading the proteins on the column, the resin was washed with 100 ml buffer (20 mM Tris-HCl [pH 7.5], 100 mM KCl, 10% glycerol, and 0.1 mM EDTA) to eliminate residual free dyes. The rest of the purification procedure was as previously described (Sun et al., 2012).

Vesicle Encapsulation of RNA Hairpin, eIF4AI, and eIF4H

Encapsulation in lipid vesicles was performed as described in Cisse et al. (2007), Okumus et al. (2004), and Rhoades et al. (2003). Lipid films were prepared by mixing 1,2-dipalmitoyl-sn-glycero-3-phosphoethanolamine-N-(Cap Biotinyl) with dimyristoyl phosphatidylcholine (DMPC) (Avanti Polar Lipids) dissolved in chloroform (1:100 molar ratio) and gently drying in vacuo. The lipids were hydrated with buffer containing 20 mM Tris–HCl (pH 7.5) and 50 mM sodium chloride. RNA substrate was incubated with eIF4AI and eIF4H at room temperature for 5 min in buffer containing 50 mM Tris-HCl (pH 7.5), 50 mM NaCl, and 2 mM $MgCl_2$. This was then mixed with lipids to yield a final concentration of 12.5 mg/ml lipid and 400 nM RNA hairpin. The mixture was manually extruded through a track-etched membrane with 200 nm holes (Whatman, GE Healthcare) more than 20 times to induce encapsulation.

smFRET Measurements of Immobilized Molecules

Total internal reflection fluorescence (TIRF) microscopy was used for single-molecule imaging of double-labeled eIF4A. We immobilized 100 pM DMPC lipid vesicles, which contained RNA hairpin, eIF4H, and double-labeled eIF4AI directly on biotinylated BSA-streptavidin coated quartz coverslip. The experimental details of imaging single molecules and data acquisition have been described previously (Sun et al., 2012). Traces were extracted and analyzed using programs written in Matlab. FRET values were calculated as $I_A/(I_A+I_D)$, where I_A and I_D are the fluorescence intensities of the acceptor and donor channels, respectively, following background and leakage correction. The two-state FRET oscillations were analyzed using hidden Markov modeling (HAMMY) (McKinney et al., 2006).

FRET Measurements of Freely Diffusing Molecules

Free diffusion smFRET measurements were carried out using a home-built laser confocal microscope system. Excitation was achieved by focusing a 532 nm laser line (New Focus) into the sample solution using a 60× 1.2 NA UPlanApo water immersion objective (Olympus). The emission part comprised a long-pass filter (Chroma HQ560LP) to remove the scattered light. The fluorescence emission was collected using the same objective, separated from the excitation light using a dichroic mirror (Chroma), and spatially filtered using a 100 μm pinhole. The emission was then spectrally split onto two APDs (PerkinElmer): one for 550–620 nm and the other for 650–710 nm. Photon counts were recorded using a counting card (PCI 6602; National Instruments) interfaced with a custom LabVIEW program. The sampling rate was 10 kHz.

FRET efficiency histograms were generated by using a two-channel data collection mode to simultaneously record donor and acceptor intensities as a function of time, with a binning time of 500 μs. The concentration of double-labeled protein used was ~20 pM, ensuring that all of the detected signals were from single molecules. The leakage of donor emission into the acceptor channel (~10%) was determined using mutant eIF4A (only one cysteine at position 66) labeled with single Cy3 dye, and then it is used to correct the signals before FRET analysis. Histograms were fitted with Gaussian functions, carrying out nonlinear least squares analysis for the fitting using Matlab (Mathworks) or Igor Pro (WaveMetrics).

SUPPLEMENTAL INFORMATION

Supplemental Information includes Supplemental Experimental Procedures and seven figures and can be found with this article online at http://dx.doi.org/10.1016/j.str.2014.04.014.

ACKNOWLEDGMENTS

We acknowledge financial support from the Human Frontiers Science Program (HFSP) (RGP0036-2005) (to A.M. and N.S.), the Israel Science Foundation (845/11) (to A.M.), and the Canadian Institutes of Health Research (CIHR) (MOP-106530) (to J.P.). L.M.L. was a NSERC Alexander Graham Bell (CGSD) fellowship recipient and currently holds a CIHR postdoctoral fellowship, a Bisby Fellowship, and a National Health and Medical Research Council Peter Doherty Early Career Fellowship.

Received: February 26, 2014
Revised: April 6, 2014
Accepted: April 24, 2014
Published: June 5, 2014

REFERENCES

Andreou, A.Z., and Klostermeier, D. (2012). Conformational changes of DEAD-box helicases monitored by single molecule fluorescence resonance energy transfer. Methods Enzymol. *511*, 75–109.

Andreou, A.Z., and Klostermeier, D. (2014). eIF4B and eIF4G jointly stimulate eIF4A ATPase and unwinding activities by modulation of the eIF4A conformational cycle. J. Mol. Biol. *426*, 51–61.

Bono, F., Ebert, J., Lorentzen, E., and Conti, E. (2006). The crystal structure of the exon junction complex reveals how it maintains a stable grip on mRNA. Cell *126*, 713–725.

Bordeleau, M.E., Mori, A., Oberer, M., Lindqvist, L., Chard, L.S., Higa, T., Belsham, G.J., Wagner, G., Tanaka, J., and Pelletier, J. (2006). Functional characterization of IRESes by an inhibitor of the RNA helicase eIF4A. Nat. Chem. Biol. *2*, 213–220.

Caruthers, J.M., Johnson, E.R., and McKay, D.B. (2000). Crystal structure of yeast initiation factor 4A, a DEAD-box RNA helicase. Proc. Natl. Acad. Sci. USA *97*, 13080–13085.

Chang, J.H., Cho, Y.H., Sohn, S.Y., Choi, J.M., Kim, A., Kim, Y.C., Jang, S.K., and Cho, Y. (2009). Crystal structure of the eIF4A-PDCD4 complex. Proc. Natl. Acad. Sci. USA *106*, 3148–3153.

Cisse, I., Okumus, B., Joo, C., and Ha, T. (2007). Fueling protein DNA interactions inside porous nanocontainers. Proc. Natl. Acad. Sci. USA *104*, 12646–12650.

Del Campo, M., and Lambowitz, A.M. (2009). Structure of the yeast DEAD box protein Mss116p reveals two wedges that crimp RNA. Mol. Cell *35*, 598–609.

Duncan, R., and Hershey, J.W. (1983). Identification and quantitation of levels of protein synthesis initiation factors in crude HeLa cell lysates by two-dimensional polyacrylamide gel electrophoresis. J. Biol. Chem. *258*, 7228–7235.

Feoktistova, K., Tuvshintogs, E., Do, A., and Fraser, C.S. (2013). Human eIF4E promotes mRNA restructuring by stimulating eIF4A helicase activity. Proc. Natl. Acad. Sci. USA *110*, 13339–13344.

Galicia-Vázquez, G., Cencic, R., Robert, F., Agenor, A.Q., and Pelletier, J. (2012). A cellular response linking eIF4AI activity to eIF4AII transcription. RNA *18*, 1373–1384.

Grohman, J.K., Del Campo, M., Bhaskaran, H., Tijerina, P., Lambowitz, A.M., and Russell, R. (2007). Probing the mechanisms of DEAD-box proteins as general RNA chaperones: the C-terminal domain of CYT-19 mediates general recognition of RNA. Biochemistry *46*, 3013–3022.

Henn, A., Cao, W., Licciardello, N., Heitkamp, S.E., Hackney, D.D., and De La Cruz, E.M. (2010). Pathway of ATP utilization and duplex rRNA unwinding by the DEAD-box helicase, DbpA. Proc. Natl. Acad. Sci. USA *107*, 4046–4050.

Jankowsky, E., and Putnam, A. (2010). Duplex unwinding with DEAD-box proteins. Methods Mol. Biol. *587*, 245–264.

Lindqvist, L., Oberer, M., Reibarkh, M., Cencic, R., Bordeleau, M.-E., Vogt, E., Marintchev, A., Tanaka, J., Fagotto, F., Altmann, M., et al. (2008). Selective pharmacological targeting of a DEAD box RNA helicase. PLoS ONE *3*, e1583.

Marintchev, A., Edmonds, K.A., Marintcheva, B., Hendrickson, E., Oberer, M., Suzuki, C., Herdy, B., Sonenberg, N., and Wagner, G. (2009). Topology and regulation of the human eIF4A/4G/4H helicase complex in translation initiation. Cell *136*, 447–460.

McKinney, S.A., Joo, C., and Ha, T. (2006). Analysis of single-molecule FRET trajectories using hidden Markov modeling. Biophys. J. *91*, 1941–1951.

O'Leary, S.E., Petrov, A., Chen, J., and Puglisi, J.D. (2013). Dynamic recognition of the mRNA cap by Saccharomyces cerevisiae eIF4E. Structure *21*, 2197–2207.

Oberer, M., Marintchev, A., and Wagner, G. (2005). Structural basis for the enhancement of eIF4A helicase activity by eIF4G. Genes Dev. *19*, 2212–2223.

Okumus, B., Wilson, T.J., Lilley, D.M., and Ha, T. (2004). Vesicle encapsulation studies reveal that single molecule ribozyme heterogeneities are intrinsic. Biophys. J. *87*, 2798–2806.

Pestova, T.V., Kolupaeva, V.G., Lomakin, I.B., Pilipenko, E.V., Shatsky, I.N., Agol, V.I., and Hellen, C.U. (2001). Molecular mechanisms of translation initiation in eukaryotes. Proc. Natl. Acad. Sci. USA *98*, 7029–7036.

Rhoades, E., Gussakovsky, E., and Haran, G. (2003). Watching proteins fold one molecule at a time. Proc. Natl. Acad. Sci. USA *100*, 3197–3202.

Richter-Cook, N.J., Dever, T.E., Hensold, J.O., and Merrick, W.C. (1998). Purification and characterization of a new eukaryotic protein translation factor. Eukaryotic initiation factor 4H. J. Biol. Chem. *273*, 7579–7587.

Rogers, G.W., Jr., Lima, W.F., and Merrick, W.C. (2001a). Further characterization of the helicase activity of eIF4A. Substrate specificity. J. Biol. Chem. *276*, 12598–12608.

Rogers, G.W., Jr., Richter, N.J., Lima, W.F., and Merrick, W.C. (2001b). Modulation of the helicase activity of eIF4A by eIF4B, eIF4H, and eIF4F. J. Biol. Chem. *276*, 30914–30922.

Roy, R., Hohng, S., and Ha, T. (2008). A practical guide to single-molecule FRET. Nat. Methods *5*, 507–516.

Sengoku, T., Nureki, O., Nakamura, A., Kobayashi, S., and Yokoyama, S. (2006). Structural basis for RNA unwinding by the DEAD-box protein Drosophila Vasa. Cell *125*, 287–300.

Shah, P., Ding, Y., Niemczyk, M., Kudla, G., and Plotkin, J.B. (2013). Rate-limiting steps in yeast protein translation. Cell *153*, 1589–1601.

Sonenberg, N., and Hinnebusch, A.G. (2009). Regulation of translation initiation in eukaryotes: mechanisms and biological targets. Cell *136*, 731–745.

Sun, Y., Atas, E., Lindqvist, L., Sonenberg, N., Pelletier, J., and Meller, A. (2012). The eukaryotic initiation factor eIF4H facilitates loop-binding, repetitive RNA unwinding by the eIF4A DEAD-box helicase. Nucleic Acids Res. *40*, 6199–6207.

Theissen, B., Karow, A.R., Köhler, J., Gubaev, A., and Klostermeier, D. (2008). Cooperative binding of ATP and RNA induces a closed conformation in a DEAD box RNA helicase. Proc. Natl. Acad. Sci. USA *105*, 548–553.

Yang, Q., Del Campo, M., Lambowitz, A.M., and Jankowsky, E. (2007). DEAD-box proteins unwind duplexes by local strand separation. Mol. Cell *28*, 253–263.

